$K^+ \to \pi^+ \nu \bar{\nu}$: First results from the NA62 experiment at CERN

Giuseppe Ruggiero
University of Lancaster, UK

Abstract

The decay $K^+ \to \pi^+ \nu \bar{\nu}$, with a very precisely predicted branching ratio of less than 10^{-10}, is one of the best candidates to reveal indirect effects of new physics at the highest mass scales. The NA62 experiment at CERN SPS is designed to measure the branching ratio of the $K^+ \to \pi^+ \nu \bar{\nu}$ with a decay-in-flight technique, novel for this channel. NA62 took data in 2016, 2017 and 2018. Statistics collected in 2016 allows NA62 to reach the Standard Model sensitivity for $K^+ \to \pi^+ \nu \bar{\nu}$, entering the domain of 10^{-10} single event sensitivity and showing the proof of principle of the experiment. The preliminary result on $K^+ \to \pi^+ \nu \bar{\nu}$ from the analysis of the 2016 data set is described.[1]

---

[1]The NA62 Collaboration: R. Aliberti, F. Ambrosino, R. Ammendola, B. Angelucci, A. Antonelli, G. Anzivino, R. Arcidiacono, M. Barbanera, A. Biagioni, L. Bician, C. Biino, A. Bizzeti, T. Blazek, B. Bloch-Devaux, V. Bonaiuto, M. Boretto, M. Bragadireanu, D. Britton, F. Brizioli, M.B. Brunetti, D. Bryman, F. Bucci, T. Capussela, A. Ceccucci, P. Cenci, V. Cerny, C. Cerri, B.

1 Introduction

The $K^+ \rightarrow \pi^+ \nu\bar{\nu}$ ($\pi\nu\nu$) is a flavour changing neutral current decay proceeding through box and electroweak penguin diagrams. A quadratic GIM mechanism and the transition of the quark top into the quark down make this process extremely rare. The Standard Model (SM) predicts [2] the branching ratio (BR) to be $(8.4 \pm 1.0) \times 10^{-11}$, where the precision on the external inputs dominates the uncertainty. The theoretical accuracy, instead, is at the level of 2%, as the SM BR includes NLO (NNLO) QCD corrections to the top (charm) quark contribution [3, 4] and NLO electroweak corrections [5]. Moreover the hadronic matrix element largely cancels when normalized to the precisely measured BR

Checcucci, A. Conovaloff, P. Cooper, E. Cortina Gil, M. Corvino, F. Costantini, A. Cotta Ramusino, D. Coward, G. D'Agostini, J. Dainton, P. Dalpiaz, H. Danielsson, N. De Simone, D. Di Filippo, L. Di Lella, N. Doble, B. Dobrich, F. Duval, V. Duk, J. Engelfried, T. Enik, N. Estrada-Tristan, V. Falaleev, R. Fantechi, V. Fascianelli, L. Federici, S. Fedotov, A. Filippi, M. Fiorini, J. Fry, J. Fu, A. Fucci, L. Fulton, E. Gamberini, L. Gatignon, G. Georgiev, S. Ghinescu, A. Gianoli, M. Giorgi, S. Giudici, F. Gonnella, E. Goudzovski, C. Graham, R. Guida, E. Gushchin, F. Hahn, H. Heath, T. Husek, O. Hutanu, D. Hutchcroft, L. Iacobuzio, E. Iacopini, E. Imbergamo, B. Jenninger, K. Kampf, V. Kekelidze, S. Kholodenko, G. Khoriauli, A. Khotyantsev, A. Kleimenova, A. Korotkova, M. Koval, V. Kozhuharov, Z. Kucerova, Y. Kudenko, J. Kunze, V. Kurochka, V.Kurshetsov, G. Lanfranchi, G. Lamanna, G. Latino, P. Laycock, C. Lazzeroni, M. Lenti, G. Lehmann Miotto, E. Leonardi, P. Lichard, L. Litov, R. Lollini, D. Lomidze, A. Lonardo, P. Lubrano, M. Lupi, N. Lurkin, D. Madigozhin, I. Mannelli, G. Mannocchi, A. Mapelli, F. Marchetto, R. Marchevski, S. Martellotti, P. Massarotti, K. Massri, E. Maurice, M. Medvedeva, A. Mefodev, E. Menichetti, E. Migliore, E. Minucci, M. Mirra, M. Misheva, N. Molokanova, M. Moulson, S. Movchan, M. Napolitano, I. Neri, F. Newson, A. Norton, M. Noy, T. Numao, V. Obraztsov, A. Ostankov, S. Padolski, R. Page, V. Palladino, C. Parkinson, E. Pedreschi, M. Pepe, M. Perrin-Terrin, L. Peruzzo, P. Petrov, F. Petrucci, R. Piandani, M. Piccini, J. Pinzino, I. Polenkevich, L. Pontisso, Yu. Potrebenikov, D. Protopopescu, M. Raggi, A. Romano, P. Rubin, G. Ruggiero, V. Ryjov, A. Salamon, C. Santoni, G. Saracino, F. Sargeni, V. Semenov, A. Sergi, A. Shaikhiev, S. Shkarovskiy, D. Soldi, V. Sougonyaev, M. Sozzi, T. Spadaro, F. Spinella, A. Sturgess, J. Swallow, S. Trilov, P. Valente, B. Velghe, S. Venditti, P. Vicini, R. Volpe, M. Vormstein, H. Wahl, R. Wanke, B. Wrona, O. Yushchenko, M. Zamkovsky, A. Zinchenko.

of the $K^+ \to \pi^0 e^+ \nu$ decay, with isospin breaking and non–perturbative effects calculated in detail [5, 6].

The $K^+ \to \pi^+ \nu \bar{\nu}$ decay is extremely sensitive to physics beyond the SM, probing the highest mass scales among the rare meson decays. The largest deviations from SM are expected in models with new sources of flavour violation, owing to weaker constraints from B physics [8, 9]. The experimental value of of the CP violating quantity ε_K limits the range of variation expected for $K^+ \to \pi^+ \nu \bar{\nu}$ BR within models with currents of defined chirality, producing also typical correlation patterns between the $K^+ \to \pi^+ \nu \bar{\nu}$ and $K_L \to \pi^0 \nu \bar{\nu}$ decay modes [10]. Present experimental constraints limit the range of variation within supersymmetric models [11, 12, 13]. The $K^+ \to \pi^+ \nu \bar{\nu}$ decay can also be sensitive to effects of lepton flavour non–universality [14] or can constrain leptoquark models [15] aiming to explain the measured CP violating ratio ϵ'/ϵ [16].

The experiments E787 and E949 at BNL [17, 18] studied the $K^+ \to \pi^+ \nu \bar{\nu}$ decay using a kaon decay–at–rest technique and measured a BR of $(17.3^{+11.5}_{-10.5}) \times 10^{-11}$. The NA62 experiment at CERN aims to measure precisely the BR of the $K^+ \to \pi^+ \nu \bar{\nu}$ decay with a novel kaon decay–in–flight technique. Here the first result of NA62 from the analysis of data collected in a data taking period in 2016 is reported, corresponding to about 5% fraction of the statistics collected by NA62 during a full–year data taking period in 2017.

2 The NA62 Experiment

The NA62 experiment is a fixed target experiment located at CERN. Fig. 1 shows a schematic view of the apparatus. NA62 adopts a kaon decay-in-flight technique. Primary SPS protons strike a target from which a secondary charged hadron beam of 75 GeV/c and 1% momentum bite is selected and transported to the decay region. The detailed descriptions of the apparatus can be found in [19]. The incoming kaon is positively identified by a differential Cerenkov counter (KTAG) and its momentum and direction are measured by three stations of Si pixel detectors (GTK). About 6% of beam particles are K^+. A guard ring detector (CHANTI) vetoes beam inelastic interactions occurring in GTK. A decay tank, holding a 10^{-6} mbar vacuum, is surrounded by lead-glass annular calorimeters (LAV) designed to catch photons up to 50 mrad. Four stations of straw chambers (STRAW) in vacuum trace downstream charged particles, with a dipole magnet providing a 270 MeV/c transverse kick for
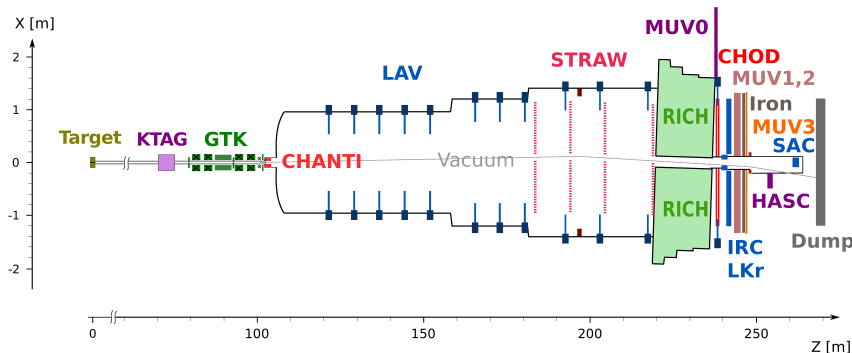
Figure 1: *Schematic layout of the NA62 experiment in the yz plane.*

momentum analysis. A RICH counter time-stamps and identifies charged particles; plastic scintillators (CHOD) are used for triggering and timing. Photon rejection in the forward region is provided by: an electromagnetic calorimeter of liquid krypton (LKr); small angle calorimeters (IRC and SAC). Hadron calorimeters (MUV1,2) and a plastic scintillator detector (MUV3) are used to suppress muons. The SPS delivers 3.3×10^{12} protons per pulse at full intensity to NA62, corresponding to 750 MHz particle rate in GTK. Information from CHOD, RICH, MUV3 and LKr are built up online to issue level zero trigger conditions. Software-based variables from KTAG, CHOD, LAV and STRAW provide higher level trigger requirements. $\pi\nu\nu$-triggered data are taken concurrently with downscaled samples of data for rare kaon decays studies and minimum bias.

The NA62 apparatus has been commissioned in 2015 and 2016. In 2016 NA62 has collected about 4.5×10^{11} kaon decays for $\pi\nu\nu$ at 20-40% of nominal intensity.

3   Principle of the Measurement

The signature of a $K^+ \to \pi^+ \nu\overline{\nu}$ decay is one K^+ in the initial state and one π^+ with missing energy in the final state. The main kinematic variable is the squared missing mass $m^2_{miss} \equiv (p_K - p_\pi)^2$, where p_K and p_π are the 4-momenta of the K^+ and π^+, respectively. The two neutrinos carry away
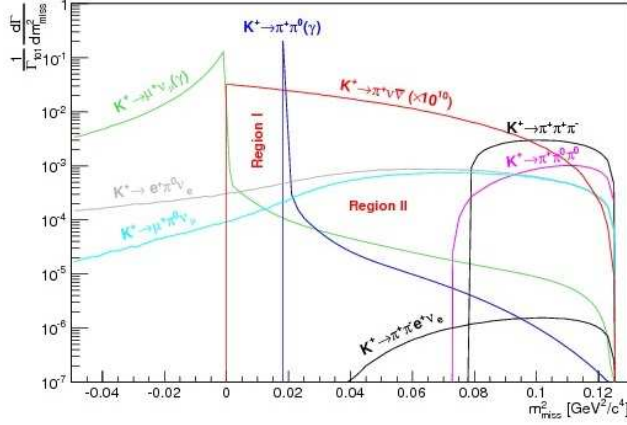
Figure 2: m^2_{miss} of K^+ decays relevant to the $K^+ \to \pi^+ \nu \bar{\nu}$ measurement. The m^2_{miss} is computed under the hypothesis that the charged particle in the final state is a π^+. Signal (red) is multiplied by 10^{10} for visibility. Two regions where to search for signal are also indicated.

a large fraction of the momentum resulting in a broadly distributed missing mass, as shown in Fig. 2. Search for signal occurs in two regions of the m^2_{miss} spectrum across the $K^+ \to \pi^+ \pi^0$ peak. Possible backgrounds are: the main K^+ decay modes $K^+ \to \pi^+ \pi^0$ and $K^+ \to \mu^+ \nu$ entering signal regions through non gaussian resolution and radiative tails of the m^2_{miss}; $K^+ \to \pi^+ \pi^+ \pi^-$ through non gaussian resolution tails; $K^+ \to l^+ \pi^0 \nu_l$ decays and more rare processes like $K^+ \to \pi^+ \pi^- e^+ \nu$ broadly distributed across the signal regions because of the neutrinos in the final state; events mimicking $K^+ \to \pi^+ \nu \bar{\nu}$ originating along the beam line via inelastic interactions of beam particles with the material; K^+s that decay before entering the fiducial volume downstream to the last station of the GTK (GTK3). Each source of background requires different rejection procedures, depending on the kinematics and on the type of charged particle in the final state. The estimation of the expected background remaining after selection is done separately for each process.

A blind procedure was adopted for the 2016 $\pi\nu\nu$ analysis, with signal and control regions kept masked as long as the evaluation of expected signal and background was not complete. The analysis makes use of data acquired with

the dedicated $\pi\nu\nu$ trigger (*PNN*) and with a minimum bias trigger (*control*).

4 Selection

The $\pi\nu\nu$ selection proceeds through: definition of a K^+ decay with a charged particle in the final state; π^+ identification; rejection of events with γ or any other activity in final state; kinematic selection and definition of the signal regions.

Signals in RICH, LKr and CHOD detectors are spatially associated to tracks reconstructed in the STRAW to identify and timestamp the π^+'s. A K^+ is identified in KTAG and traced in GTK. The K^+ is matched to the candidate π^+ exploiting the $\mathcal{O}(100 \text{ ps})$ time coincidence resolution between KTAG, GTK and RICH and the $\mathcal{O}(\text{mm})$ resolution of the closest distance of approach between the STRAW and GTK tracks. An about 50 m long fiducial decay region for $K^+ \rightarrow \pi^+ \nu\bar{\nu}$ is chosen, starting from about 10 m downstream of the last GTK station. The selection of K^+ decays in this region makes use of criteria based on: reconstructed decay vertex, π^+ position extrapolated back at the entrance of the fiducial region, π^+ emission angle, extra-activity in CHANTI and GTK.

The $\pi\nu\nu$ analysis is restricted to $15 < P_{\pi^+} < 35$ GeV/c. This cut costs half of the signal acceptance, but improves significantly the π^0 detection and exploits the optimal range for π^+ identification and $K^+ \rightarrow \mu^+ \nu$ rejection.

Calorimeters and RICH provide π^+ identification against μ^+ and positrons. A multi-variate classifier combines calorimetric information. RICH variables are used to build: a STRAW track-based likelihood discriminant; the mass of the particle using the momentum measured by the STRAW; the momentum of the particle assuming the π^+ mass. Achieved performances for π^+ momentum between 15 and 35 GeV/c are: 0.6×10^{-5} (78%) μ^+ (π^+) efficiency with calorimeters, 2.1×10^{-3} (82%) μ^+ (π^+) efficiency with RICH.

The LAV, LKr, IRC and SAC ensure rejection of photons with direction from 0 up to 50 mrad with respect to the beam axis. The time coincidence between extra energy in these detectors and π^+ is the main veto condition and typical veto time windows range from ± 3 to ± 10 ns. Further selection criteria based on extra activity in CHOD's and STRAW, called multiplicity rejection, are employed against photons interacting with material upstream of photon vetoes and losing energy either in the beam pipe or through hadron production.
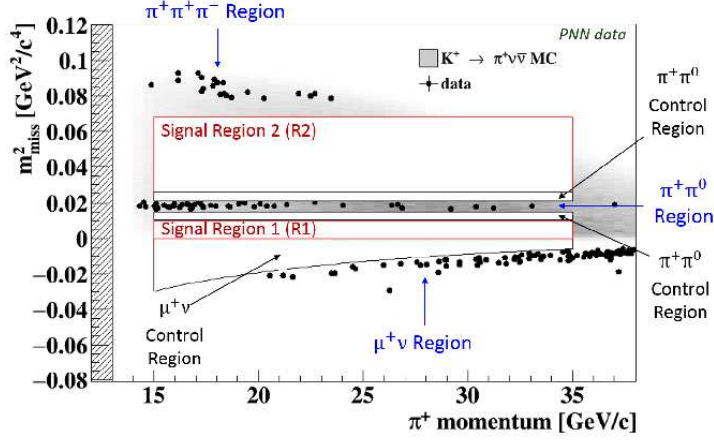
Figure 3: m_{miss}^2 as a function of $P_{\pi+}$ for PNN trigger data events (dots) passing the $\pi\nu\nu$ selection, but the cuts on m_{miss}^2 and $P_{\pi+}$. Grey area corresponds to the distribution of $\pi\nu\nu$ MC events, with darker (lighter) grey indicating more (less) populated regions. Red (black) lines define the signal (control) regions and are masked. Three background regions are also shown.

Multiplicity rejection is also effective against decays like $K^+ \to \pi^+\pi^+\pi^-$ and $K^+ \to \pi^+\pi^-e^+\nu$. The achieved π^0 detection inefficiency is about 2.5×10^{-8}, measured on data.

The invariant $m_{miss}^2 \equiv (p_{K^+} - p_{\pi+})^2$ is used to discriminate between the signal and background kinematics, where p_{K^+} ($p_{\pi+}$) is the K^+ (π^+) 4-momenta measured by the GTK (STRAW) under the hypothesis of the K^+ (π^+) mass. Fig. 3 shows the distribution of the remaining events in the ($m_{miss}^2 - P_{\pi+}$) plane, with $P_{\pi+}$ the magnitude of the π^+ 3-momentum. This plane defines three background regions mostly populated by $K^+ \to \pi^+\pi^0$, $K^+ \to \mu^+\nu$ and $K^+ \to \pi^+\pi^+\pi^-$ decays; signal regions below and above the $K^+ \to \pi^+\pi^0$ called *Region 1* and *2*, respectively; three control regions between the signal and the $K^+ \to \pi^+\pi^0$ and $K^+ \to \mu^+\nu$ regions. The 10^{-3} GeV^2/c^4 m_{miss}^2 resolution of the $K^+ \to \pi^+\pi^0$ peak drives the choice of the boundaries of these regions. The same m_{miss}^2 is also computed taking $P_{\pi+}$ measured with the RICH instead of the STRAW or assuming the nominal K^+ momentum and direction instead of the GTK measurements. Constraints on these variables are also applied

to define signal regions, providing additional power to suppress background coming from tracks mis-reconstructed in STRAW or GTK.

5 Single Event Sensitivity

The single event sensitivity SES is defined as $1/(N_K \cdot \varepsilon_{\pi\nu\nu})$, where N_K is the number of K^+ decays and $\varepsilon_{\pi\nu\nu}$ is the signal efficiency for the $K^+ \to \pi^+\nu\bar{\nu}$ selection. The number N_K is $(1.21 \pm 0.02_{syst}) \times 10^{11}$, measured using a sample of $K^+ \to \pi^+\pi^0$ and computed as $(N_{\pi\pi} \cdot D)/(A_{\pi\pi} \cdot BR_{\pi\pi})$. Here $N_{\pi\pi}$ is the number of $K^+ \to \pi^+\pi^0$ decays selected on control data using the same $K^+ \to \pi^+\nu\bar{\nu}$ criteria, except the γ, the multiplicity rejection and the cut on m^2_{miss}; $A_{\pi\pi}$ their selection acceptance estimated to be about 10% using a MC simulation; $BR_{\pi\pi}$ and $D = 400$ are the branching ratio of the $K^+ \to \pi^+\pi^0$ decay and the downscaling factor of the control trigger, respectively. Discrepancies in data/MC agreement and variation of the measured K^+ flux as a function of P_{π^+} are the main sources of systematic uncertainty to N_K.

The signal efficiency is computed separately in four bins of P_{π^+}, 5 GeV/c wide, as the product of three terms, $(A_{\pi\nu\nu} \cdot \epsilon_{RV} \cdot \epsilon_{trig})$. $A_{\pi\nu\nu}$ is the $K^+ \to \pi^+\nu\bar{\nu}$ selection acceptance extracted from MC; ϵ_{RV} the signal efficiency due to losses resulting from γ and multiplicity rejection induced by the random activity in the detectors; ϵ_{trig} the PNN trigger efficiency. Additional sources of event loss common both to $K^+ \to \pi^+\nu\bar{\nu}$ and $K^+ \to \pi^+\pi^0$ are not accounted for as they cancel in the signal to normalisation ratio entering SES.

The selection acceptance $A_{\pi\nu\nu}$ is about 4% overall (Fig. 4, a). Trigger efficiency is measured using control data and $K^+ \to \pi^+\pi^0$ control samples and is about 88%, weakly dependent on P_{π^+}, with losses due mainly to the LKr and MUV3 veto conditions. Random veto efficiency ϵ_{RV} is estimated on data using a sample of $K^+ \to \mu^+\nu$ candidates and corresponds to $\epsilon_{RV} = 0.76 \pm 0.04$, where the uncertainty comes from the estimation of the losses induced by the π^+ interactions. The random veto efficiency is flat as a function of P_{π^+}, but depends on the intensity (Fig, 4, b).

The final measured SES and the corresponding number of SM $K^+ \to \pi^+\nu\bar{\nu}$ expected in signal regions 1 and 2 are:

$$SES = (3.15 \pm 0.01_{stat} \pm 0.24_{syst}) \times 10^{-10}, \tag{1}$$

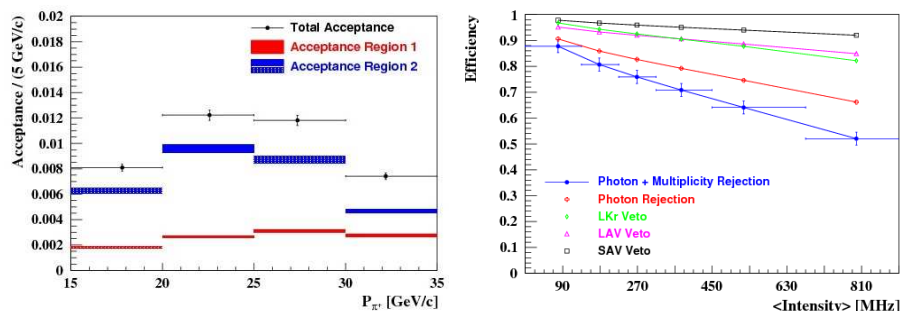$$N^{exp}_{\pi\nu\nu}(SM) = 0.267 \pm 0.001_{stat} \pm 0.020_{syst} \pm 0.032_{ext}. \tag{2}$$

Figure 4: *a)* $A_{\pi\nu\nu}$ *per bins of* P_{π^+} *in regions 1+2 (dots) with total uncertainty and in regions 1, 2 (red, blue boxes) separately with total uncertainty (vertical box size). b) signal efficiency in bins of beam intensity after photon and multiplicity rejection due to the random activity with total uncertainty (blue dots), after photon rejection (red crosses), after IRC and SAC veto only (black square), after LAV veto only (pink triangle), after LKr only (green diamond). Lines are for eye guidance. Out–of–time activity in GTK is used to estimate the event–by–event intensity.*

The external error to $N_{exp}^{\pi\nu\nu}(SM)$ comes from the uncertainty on the SM $K^+ \to \pi^+\nu\bar{\nu}$ branching ratio. The systematic uncertainty on SES mostly comes from ϵ_{RV} and $A_{\pi\pi}$ and is propagated to $N_{\pi\nu\nu}^{exp}$.

6 Background estimation

Background from K^+ decaying in the fiducial region comes primarily from $K^+ \to \pi^+\pi^0$, $K^+ \to \mu^+\nu$, $K^+ \to \pi^+\pi^+\pi^-$ and $K^+ \to \pi^+\pi^-e^+\nu$.

Kineatic thresholds limit the m_{miss}^2 spectrum of $K^+ \to \pi^+\pi^0$, $K^+ \to \mu^+\nu$ and $K^+ \to \pi^+\pi^+\pi^-$. To estimate the fraction of these decays remaining in signal regions, the assumption is made that π^0 rejection for $K^+ \to \pi^+\pi^0$, particle identification for $K^+ \to \mu^+\nu$ and multiplicity rejection for $K^+ \to \pi^+\pi^+\pi^-$ are independent from the m_{miss}^2 cuts defining the signal regions. The number of expected events in signal regions from these processes, $N_{background}^{exp}$, is computed as $N(background) \cdot f^{kin}$; here $N(background)$ is the number of remaining PNN triggered events in the corresponding background region after the $\pi\nu\nu$ selection, but the cut on m_{miss}^2; f^{kin} is the fraction of background
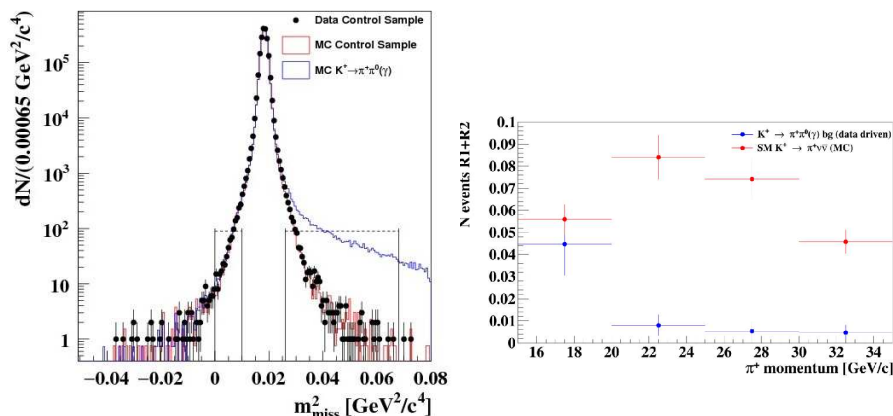
Figure 5: *a)* m_{miss}^2 *distribution of the* $K^+ \to \pi^+\pi^0(\gamma)$ *control events selected on data tagging the* π^0 *(dots). Two* $K^+ \to \pi^+\pi^0(\gamma)$ *MC samples are superimposed: one selected as in data (red line), the other selected as* $\pi\nu\nu$ *(blue line, referred as MC* $K^+ \to \pi^+\pi^0(\gamma)$ *in the legend). The region between the two vertical lines joined by the dotted horizontal line at* m_{miss}^2 *lower (higher) than the* $m_{\pi^0}^2$ *peak indicates region 1 (2). b) expected* $K^+ \to \pi^+\pi^0(\gamma)$ *background in bins of* P_{π^+} *compared to the expected number of SM* $K^+ \to \pi^+\nu\bar{\nu}$ *events.*

events entering signal regions through the reconstructed tails of the corresponding m_{miss}^2 peak. The fraction f^{kin}, called *tails*, is modeled on control samples selected on data and eventually corrected for biases induced by the selection criteria using MC simulations. The above procedure is applied separately in four bins of P_{π^+} for $K^+ \to \pi^+\pi^0$ and $K^+ \to \mu^+\nu$. Expected background in control regions is derived similarly.

The reconstruction tails of the $K^+ \to \pi^+\pi^0$ m_{miss}^2 distribution are studied from a $K^+ \to \pi^+\pi^0$ control sample selected tagging the π^0 with two γ's in LKr. Simulations accurately reproduces the tails over 4–5 orders of magnitudes (Fig, 5, a). The π^0 tagging does not bias the resolution tails of $K^+ \to \pi^+\pi^0$, but suppresses almost completely the radiative part coming from $K^+ \to \pi^+\pi^0\gamma$ decays. This radiative contribution is estimated using MC simulation and the measured single photon detection efficiency of the different photon vetoes. The background from $K^+ \to \pi^+\pi^0$ and from its radiative process integrated over bins of P_{π^+} is summarised in Tab. 1. The background depends on P_{π^+} as
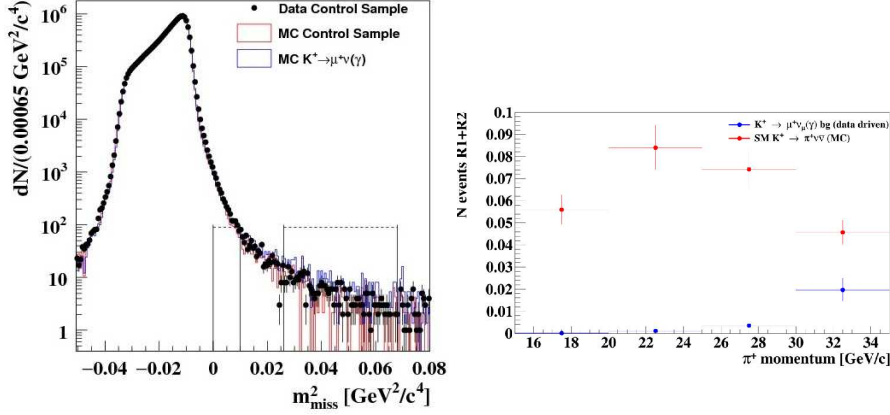
Figure 6: *a) m_{miss}^2 distribution of the $K^+ \to \mu^+\nu(\gamma)$ control events selected on data (dots) with two MC $K^+ \to \mu^+\nu(\gamma)$ samples superimposed: one selected as in data (red line), the other selected as $\pi\nu\nu$ without particle identification (blue line, referred as MC $K^+ \to \mu^+\nu(\gamma)$ in the legend). The two regions between the two vertical lines joined by the dotted horizontal line correspond to region 1 and 2 (lower and higher m_{miss}^2, respectively). b) expected $K^+ \to \mu^+\nu(\gamma)$ background in bins of P_{π^+} compared to the expected number of SM $K^+ \to \pi^+\nu\bar{\nu}$ events.*

residual PNN trigger events in $\pi^+\pi^0$ region gather at low P_{π^+} (Fig. 5, b). After un-blinding the $K^+ \to \pi^+\pi^0$ control regions, one event is observed while $1.46 \pm 0.16_{stat} \pm 0.06_{syst}$ are expected.

Reconstruction tails of $K^+ \to \mu^+\nu$ are modeled by a control sample selected identifying the μ^+. Comparisons between data and MC suggest that tails are accurately simulated over 5 orders of magnitude (Fig. 6, a). The bias induced by the μ^+ identification is assigned as systematic uncertainty. The radiative contribution is included in the measured tails. Effects of possible correlation between the RICH π^+ identification and the m_{miss}^2 are studied on data and a corresponding systematic uncertainty assigned to the expected $K^+ \to \mu^+\nu$ background. The final expectation integrated over P_{π^+} is summarised in Tab. 1. The background depends on P_{π^+} as both tails and particle identification increase at higher momenta as a consequence of $K^+ \to \mu^+\nu$ kinematics and RICH performances, respectively (Fig. 6, b). After un-blinding the $K^+ \to \mu^+\nu$ control region, two events are observed while $1.02 \pm 0.16_{stat}$ are
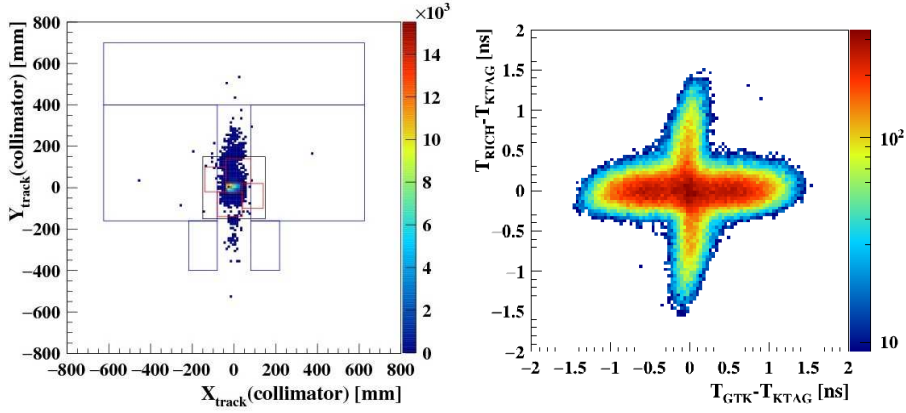
Figure 7: *a) position at the entrance of the fiducial region of π^+'s from a data sample enriched for upstream events. Blue lines correspond to the contour of the dipole before GTK3; red lines show the contour of the final collimator; black line indicate the acceptance region covered by CHANTI. b) time difference between RICH and KTAG versus GTK and KTAG for the same π^+'s of plot a).*

expected.

The $K^+ \to \pi^+\pi^+\pi^-$ decays could enter primarily region 2. The expected background is evaluated similarly to $K^+ \to \pi^+\pi^0$ and $K^+ \to \mu^+\nu$. Multiplicity rejection and kinematic cuts turn out to be very effective against $K^+ \to \pi^+\pi^+\pi^-$ decays and the expected background is found to be almost negligible (Tab. 1).

Background from $K^+ \to \pi^+\pi^-e^+\nu$ (K_{e4}) is expected in signal region 2. It is suppressed by multiplicity rejection, particle identification, kinematics and by the branching ratio [16] of 4.25×10^{-5}. As the K_{e4} kinematics is strongly correlated to the topology, the corresponding background (Tab. 1) is estimated using a MC sample of 4×10^8 simulated decays, validated on data using different K_{e4} enriched selections, orthogonal to $\pi\nu\nu$.

Considerations based on selection performances (Section 4) show that background from $K^+ \to e^+\pi^0\nu$, $K^+ \to \mu^+\pi^0\nu$ and $K^+ \to \pi^+\gamma\gamma$ decays is negligible.

Process	Expected events in signal regions
$K^+ \to \pi^+\pi^0(\gamma)$	$0.064 \pm 0.007_{stat} \pm 0.006_{syst}$
$K^+ \to \mu^+\nu(\gamma)$	$0.020 \pm 0.003_{stat} \pm 0.003_{syst}$
$K^+ \to \pi^+\pi^-e^+\nu$	$0.018^{+0.024}_{-0.017}|_{stat} \pm 0.009_{syst}$
$K^+ \to \pi^+\pi^+\pi^-$	$0.002 \pm 0.001_{stat} \pm 0.002_{syst}$
Upstream Background	$0.050^{+0.090}_{-0.030}|_{stat}$
Total Background	$0.15 \pm 0.09_{stat} \pm 0.01_{syst}$

Table 1: *Summary of the background estimation from the $\pi\nu\nu$ analysis of 2016 data. Here $K^+ \to \pi^+\pi^0(\gamma)$ ($K^+ \to \mu^+\nu(\gamma)$) stays for $K^+ \to \pi^+\pi^0$ ($K^+ \to \mu^+\nu$) plus $K^+ \to \pi^+\pi^0\gamma$ ($K^+ \to \mu^+\nu\gamma$) decays.*

In addition to K^+ decays in the fiducial region, backgrounds can originate from upstream events classified as π^+ from:

1. K^+ decays upstream of the decay region, most notably between GTK stations 2 and 3, matched to a pileup beam particle;

2. interactions of a beam π^+ mostly with GTK station 3, but also with station 2, matched to a pileup K^+;

3. interactions of a K^+ with material in the beam, produced either as prompt particle originating from the interaction or as a decay product of a neutral kaon.

The interpretation of the upstream events in terms of the above topologies is supported by a closer look to a $\pi\nu\nu$-like data sample enriched for upstream events. The position of the π^+ mesons at the entrance of the fiducial region (Fig. 7, a) indicates their origin upstream or via interactions in GTK stations and drives the choice of a geometrical cut covering the central aperture of the dipole (box cut defined by $|X_{track}| < 100$ mm and $|Y_{track}| < 500$ mm); the distribution of the time coincidence between KTAG-RICH and GTK-KTAG suggests an accidental source for these events (Fig. 7, b). The estimation of the upstream background is made on data using a purely data–driven method and is shown in Tab. 1, where The statistics of the data samples limits the accuracy of the final value.

Summing up the various the contributions, the overall final expected background in region 1 and 2 is $0.15 \pm 0.09_{stat} \pm 0.01_{syst}$ (Tab. 1).
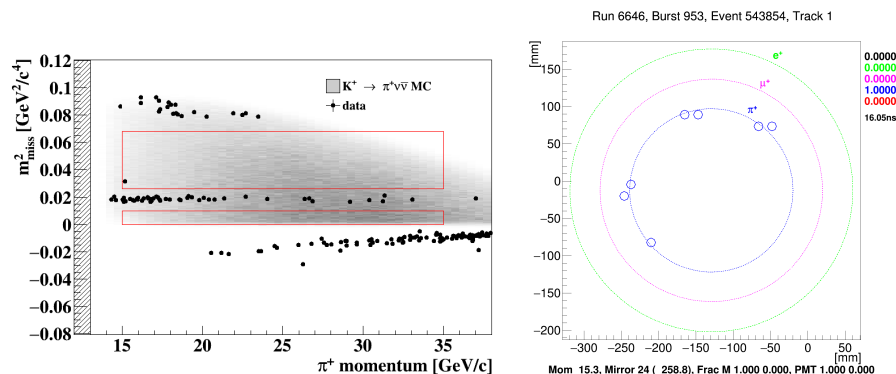
Figure 8: *a)* m^2_{miss} *as a function of* P_{π^+} *for PNN trigger data events (dots) passing the* $\pi\nu\nu$ *selection, but the cuts on* m^2_{miss} *and* P_{π^+}*. The grey area corresponds to the distribution of* $\pi\nu\nu$ *MC events. Red lines define the signal regions. The event observed in region 2 is shown. b) position of the hits in the RICH forming the ring associated to the* π^+ *of the observed event in region 2, as given by the RICH event display. The circles illustrate the positron, muon and pion hypothesis, showing a perfect agreement of the observed event with the pion hypothesis.*

7 Result

After un-blinding the signal regions, one event is found in region 2, as shown in Fig. 8 (a). The corresponding π^+ has a momentum of 15.3 GeV/c. The RICH clearly indicates that it is a pion (Fig. 8, b).

The statistical model is that of a counting experiment with the expected signal in Sec. 5 and the expected background in Tab. 1. The hybrid frequentistic–bayesian prescription described in [20] is applied to account for the uncertainty on the expected background. Using the CL_s method [21], the observed upper limit on the $K^+ \to \pi^+ \nu\bar{\nu}$ branching ratio is

$$BR(K^+ \to \pi^+ \nu\bar{\nu}) < 14 \times 10^{-10} \text{ @ 95\% CL,} \tag{3}$$

where expected limits is $BR(K^+ \to \pi^+ \nu\bar{\nu}) < 10 \times 10^{-10}$.

8 Conclusions

The first search for the decay $K^+ \to \pi^+ \nu \bar{\nu}$ with kaon decays in-flight is reported. The data collected in 2016 amount to about 1% of the total exposure of the NA62 experiment in 2016-2018. The SES is found to be 3×10^{-10}. The analysis has revealed one candidate event compatible with the SM expectation (0.27) and with the background expectation (0.15). Interpreting the candidate as background leads to the upper limit 14×10^{-10} at 95% CL on the $K^+ \to \pi^+ \nu \bar{\nu}$ branching ratio. The NA62 experiment has already collected more than 20 times the statistics presented here and the analysis of this larger data sample is in progress.

References

1. J.H. Christenson *et al*, Phys. Rev. Lett. **13**, 138 (1964).

2. A. J. Buras, D. Buttazzo, J. Girrbach–Noe and R. Knegjens, JHEP 1511 (2015) 33.

3. G. Buchalla and A. J. Buras, Nucl. Phys. B 548 (1999) 309.

4. A. J. Buras, M. Gorbhan, U. Haisch and U. Nierste, JHEP 11 (2006) 002.

5. J. Brod, M. Gorbahn and E. Stamou, Phys. Review D 83 (2011) 034030.

6. G. Isidori, F. Mescia and C. Smith, Nucl. Phys. B 718 (2005), 319.

7. F. Mescia and C. Smith, Phys. Review D 76 (2007), 034017.

8. M. Blanke, A.J. Buras and S. Recksiegel, Eur. Phys. J. C 76 (2016) no.4, 182.

9. M. Blanke, A. J. Buras, B. Duling, K. Gemmler and S. Gori, JHEP 0903 (2009) 108.

10. A.J. Buras, D. Buttazzo and R. Knegjens, JHEP 1511 (2015) 166.

11. G. Isidori, F. Mescia, P. Paradisi, C. Smith and S. Trine, JHEP 0608 (2006) 064.

12. T. Blazek and P. Matak, Nucl. Phys. Proc. Suppl. 198 (2010) 216.

13. M. Tanimoto and K. Yamamoto, PTEP 2016 (2016) no.12 123B02.

14. M. Bordone, D. Buttazzo, G. Isidori and J. Monnard, Eur. Phys. J. C 77 (2017) no.9 618.

15. C. Bobeth and A. J. Buras, JHEP 1802 (2018) 101.

16. C. Patrignani *et al*, Particle Data Group, Chin. Phys. C 40 (2016) 100001.

17. A.V. Artamonov *et al*, Phys. Rev. Lett. 101 (2008) 191802.

18. A.V. Artamonov *et al*, Phys. Rev. D 79 (2008) 092004.

19. E. Cortina Gil *et al*, J. Instrum. 12 (2017) P05025.

20. R.D. Cousins, et al., Nucl. Instrum. Methods A 529 (2008) 480.

21. A.L. Read, J. Phys. G 28 (2002) 2693.